the TMZ-treated spheroids (n=12) (1week, p-value=0.003 and 2 weeks p-value<0.00002, respectively, Student's t-test) (Figure 3G). In 3D-T98G cells, a statistically significant increase in size was recorded at 1 and 2 weeks for both control (n=12) (p =0.0001, Student's t-test) and TMZ-treated spheroids (n=12) (p =0.001, p <0.00002, respectively, Student's t-test), confirming their resistance to TMZ treatment (Figure 3H). Ki67 real-time expression analysis at 2 weeks after TMZ treatment confirmed the FLIM readouts and size results (p =0.002. Student's t-test) (Figure 3I).

FLIM metabolic imaging of TMZ treated patient-derived GB-EXPs

Using the methodological criteria set by the supporting technical experiments on GB cell lines, we assessed the TMZ response in 21 glioblastoma patient-derived tumors. For each patient, GB-EXPs with similar dimensions between 70 and 200μm for drug testing, and a minimum of 14 to a maximum of 33 explants were analyzed (Supplementary Table 4). The GB-EXPs of the tumor case in Figure 4A show overlapping fractional NAD(P)H mean distribution curves between the treated (red) and control (blue) explants, which is indicative of an identical distribution of bound and free NAD(P)H (12) (Figure 4B) with a 0%DR. In Figures 4C, D, we report examples of GB-EXPs derived from the GB15 case, resulting in distinctive phasor maps. NAD(P)H fractional mean distribution curves were also distinguishable between the control and treated cases. The distribution curves (Figures 4E, F) showed a statistically significant shift of the red curves towards more abundant bound NAD(P)H molecular species in TMZ-treated explants compared to the control ones, with 59.3%DR (Figure 4E) and 90.9%DR (Figure 4F), corresponding to 24 and 72 h TMZ treatment, respectively (Supplementary Table 5). Larger amounts of bound-state NAD(P)H reflect oxidative metabolism, which is typical of less proliferative cells (10, 13) and therefore a responsive tumor.

Overall, to assess the final annotation of TMZ Responder (Resp) or Non Responder (Non-Resp), we calculated for each case a Final %DR to TMZ treatment (see Materials and Methods), as shown in Figure 4G (green-red color scale), leading us to stratify our tumor samples into 11 Non-Resp (% DR<5) and 10 Resp. The Resp group was further subdivided into several categories: Low Responders (LR) (5≤%DR<20), Medium Responders (MR) (20≤%DR<50), and High Responders (HR) (%DR≥50) (Figure 4G). It is noteworthy to point out that between core and peripheral portions of the 5 GB tumor cases included in the dataset, we observed a different drug response behavior (Supplementary Figure 4). As expected, GB2, GB3, and GB4 core regions showed a more drug-resistant behavior compared to peripheral tumor portions (28) in particular, GB2c was assessed as MR and GB2p as HR, while GB3c/4c were NR and GB3p/4p were LR. GB6c/p and GB7c/p were both assessed as Non-Resp (Figure 4G).

To corroborate the FLIM-based metabolic imaging drug efficacy predictions in stratifying samples in Resp and Non-Resp, we performed a size analysis on all 21 sample-derived GB-EXPs. Images were acquired at 0, 1, and 2 weeks for both control and TMZ-treated cases for a minimum of 15 to a maximum of 81 GB-EXPs per sample (Supplementary Table 4). The examples reported in Figure 3H show a clear reduction in size for the Resp GB-EXP compared to the Non-Resp. Overall, the area measurement of the GB-EXPs Resp group revealed a statistically significant decrease at 1 and 2 weeks after TMZ treatment (p=0.0002 and p<0.0001, respectively; Student's t-test), thus supporting the FLIM-based metabolic imaging predictions (Figure 4I).

To further support our results, we measured the changes in Ki67 mRNA expression 2 weeks after TMZ treatment. Differential analysis of Ki67 expression was performed on seven Non-Resp and eight Resp samples. Ki67 mRNA expression was significantly reduced in the Resp group after TMZ treatment compared to that in the controls, indicating a lower proliferation rate (p=0.003, Student's t-test). (Figure 4J). No significant difference was found in the Non-Resp group.

In accordance with what has been reported in the clinic and in the literature (29), we observed a higher percentage of methylated cases (77%) in the Resp tumor group than in the Non-resp tumor group (45%) (Figure 4K).

Genome-wide analyses

We performed next-generation sequencing analyses to characterize the genetic background of the Resp and Non-Resp tumors to establish a correlation between the TMZ response phenotype identified by our FLIM approach and the underlying molecular profile.

Whole transcriptome analysis (WTA)

WTA was performed on nine Resp and nine Non-Resp samples, including the cases provided with a core and a peripheral portion. Differential expression analysis identified 42 statistically significant genes between the two experimental groups (Supplementary Table 6). In Figure 5A, a heatmap analysis was initially run excluding the peripheral tumor portions to avoid repeated measures derived from similar genetic backgrounds with their core counterparts. Results showed that seven Resp and seven Non-Resp samples perfectly clustered on the basis of the 42 gene expression levels, supporting that distinct TMZ responsive and non-responsive phenotypes are well reflected at the molecular level. Among the 42 genes (Supplementary Table 6), we identified several genes involved in the TMZ response that are worth mentioning. The EGFR gene, which showed a significant

10.3389/fonc.2022.969812

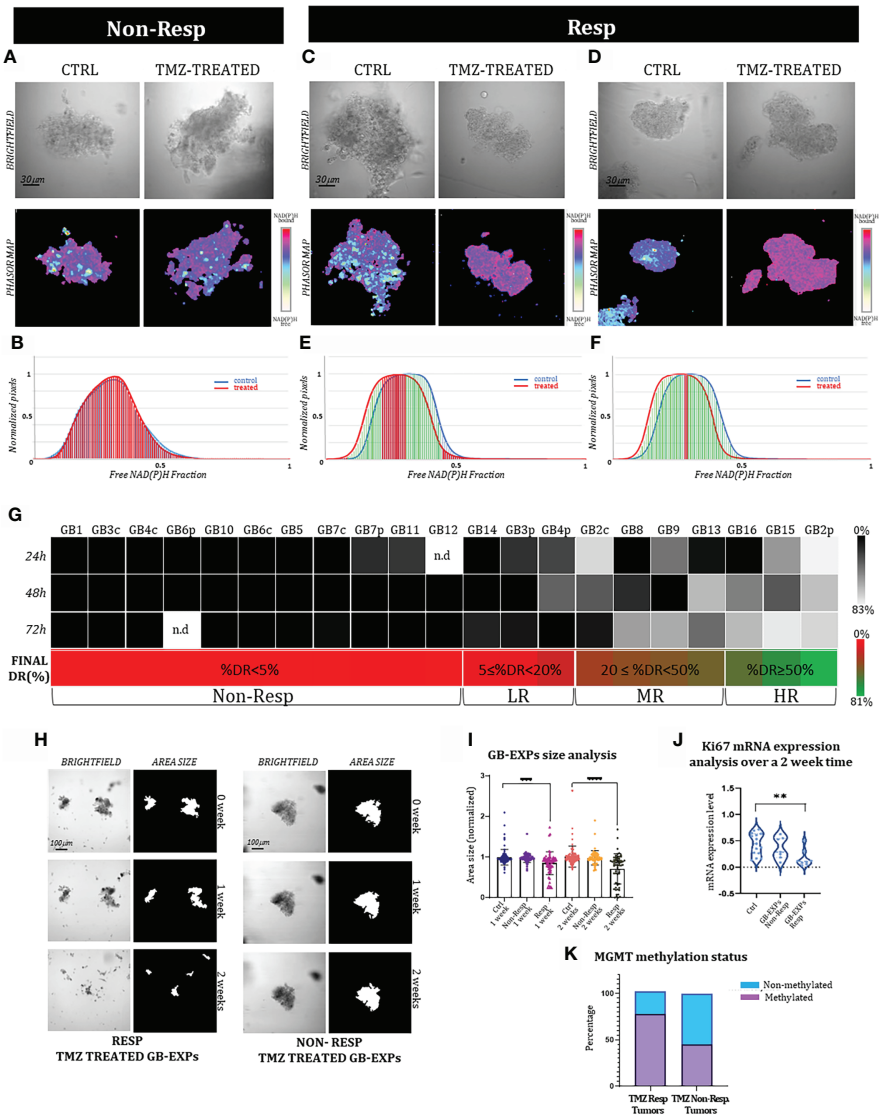

FIGURE 4
FLIM-based metabolic imaging on GB-EXPs. **(A, C, D)** 72 hr post-treatment one Non-Resp and two Resp tumor derived GB-EXPs are shown including a brightfield image and the corresponding phasor map. **(B)** In the Non-Resp case **(A)** NAD(P)H fractional mean distribution curves (72hrs) overlap between control (blue) and treated GB-EXPs (red) **(B)**. **(E, F)** NAD**(P)**H fractional mean distribution curves show a left-bound shift of the red curves (treated GB-EXPs). **(G)** %DR at 24, 48, and 72 hr, represented by a grey scale is shown for each GB case. The annotation of Resp and Non-Resp was assigned on the basis of the Final %DR, obtained from the weighted average of the 3 time points (shown with a green-red color bar for each GB case). Samples are further subdivided based on Final %DR into several categories. **(H)** Representative brightfield and area size images of a Resp and of a Non-Resp case-derived GB-EXP in matrigel at 0, 1 and 2 weeks. **(I)** Size analysis of Controls, Resp and Non-Resp patients-derived GB-EXPs (n=215, n=130, n=124 respectively) at 1 and 2 weeks. A statistically significant decrease at 1 and 2 weeks ($p=0.0002$; $p<0.0001$, respectively; Student's t test) is shown for the Resp group. **(J)** Ki67 mRNA expression using ddPCR in Resp (n=8) and Non Resp (n=7) cases after 2 weeks of TMZ treatment (*$p=0.003$, Student's t test). **(K)** MGMT promoter methylation status in Resp (n=9) and Non Resp (n=11) cases. Asterisks indicate level of statistical significance.

downregulation in Non-Resp samples, is consistent with literature data showing that glioblastoma TMZ-resistant cell lines lack EGFR activation and expression (30). Our results are, as well, confirmed for the upregulation of the CA9 gene in the Non-Resp group, the inhibition of which enhances the sensitivity of glioma cells to TMZ treatment, and highlights the value of developing small molecules or antibodies against the CA9 pathway, for combination therapy with TMZ (31) (Supplementary Table 9; Figure 5A). In the Non-Resp group, we identified downregulation of the FGFR3 gene, which is associated with a poor response to TMZ treatment (32). The same authors reported that a combination treatment of

10.3389/fonc.2022.969812

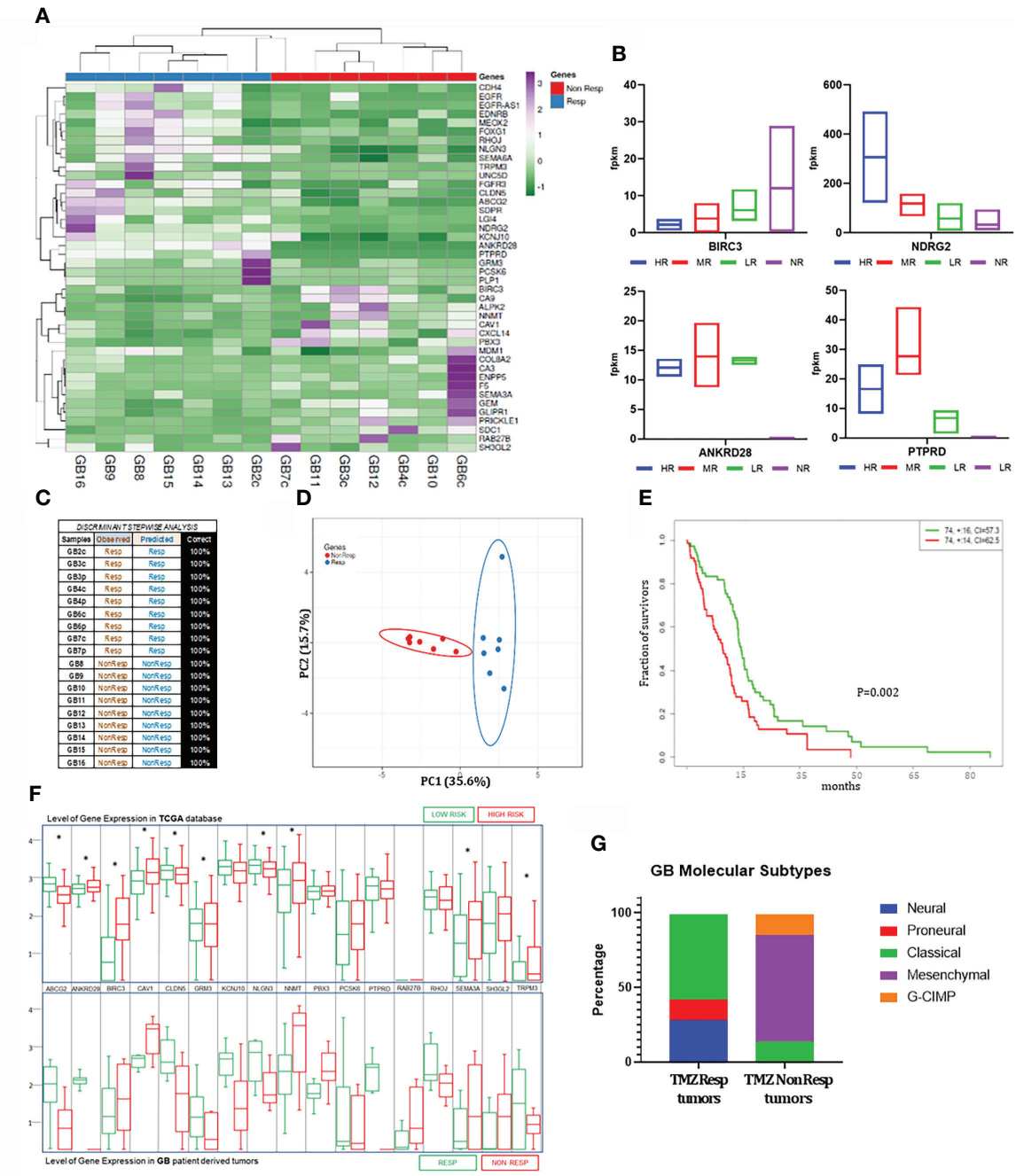

FIGURE 5
Gene expression profiling of GB-EXPs. **(A)** Heatmap of 42 genes from RNAseq data differentially expressed (DE) between Resp (n=7) and Non-Resp (n=7 (tumor peripheral portions were excluded). **(B)** Expression levels of 4 genes subdivided in HR (n=2), MR (n=4), LR (n=3) and NR (n=9) groups (peripheral portions were included). **(C)** Stepwise discriminant analysis identifies a combination of 17 DE genes that discriminates the Resp (n=9) and Non-Resp (n=9) cases with 100% accuracy (peripheral portions were included). **(D)** PCA showing RNAseq data of 17 DE genes in 7 Resp and 7 Non-Resp (tumor peripheral portions were excluded. **(E)** The 17 gene panel Kaplan-Meier plot that identifies a TCGA Low-Risk and High-Risk survival group. Concordance Index = 64.34, Log–Rank Equal Curves p=0.001853, R^2 = 0.192/0.998 Risk Groups Hazard Ratio = 1.79 (conf. int. 1.23 ~ 2.6), p=0.002172. **(F)** Expression levels of the 17 discriminant genes in TCGA database (in the top) and in GB tumors (9 Resp and 9 Non-Resp. in the bottom). **(G)** Molecular subtypes of GB samples in Resp (n=7) and Non-Resp (n=7) groups. Asterisks indicate level of statistical significance.

vinblastine (VBL) and mebendazole (MBZ) with TMZ was more effective in reducing the cell number when glioblastoma cells had low expression levels of FGFR3. Most noteworthy are the genes that we report in Figure 5B, BIRC3 and NDRG2, which show differential gene expression that varies gradually according to %DR, supporting phasor-NAD(P)H FLIM drug response stratification. Some studies in 2016 and 2021 (33, 34) report that BIRC3 gene was found expressed at a higher level in recurrent GB than in newly diagnosed GB and emerged as a novel driver of TMZ therapeutic resistance, suggesting that, during TMZ therapy, concurrent BIRC3-specific inhibition could be exploited for enhanced benefit. NDRG2 showed an opposite trend compared to BIRC3 (Figure 5B). The main mechanism underlying NDRG2 silencing in gliomas remains unknown. There is also debate on whether NDRG2 gene activity reflects the survival of glioma patient (35). Furthermore, we identified two genes that were completely silenced in all samples of the Non-Resp group, ANKRD28 and PTPRD (Figures 5A, B). In the GB3c,p and 4c,p composed of a core and peripheral portion with different response to TMZ treatment (Figure 4G), both genes resulted differentially expressed always in accordance with their phenotype. Non-responsive tumor portions had consistently complete loss of ANKRD28 and PTPRD expression unlike their responsive counterparts (Figures 4G, 5B). While the ANKRD28 gene has an unknown role in GB, the tyrosine phosphatase PTPRD is a tumor suppressor that is frequently inactivated and mutated in GB and other human cancers (36).

Finally, on the 42 significant genes, we performed a stepwise discriminant analysis that enabled the identification of a 17 gene signature (Supplementary Table 6), which could discriminate the Resp and Non-Resp tumor samples with 100% accuracy (Figures 5C, D). To investigate the potential disease course of patients whose tumors we had predicted to respond to TMZ, we queried the TCGA database of hundreds of clinically and molecularly characterized GB patients. Therefore, the 17 gene profile was used in the "SurvExpress Biomarker Validation of Cancer Gene Expression" tool, to interrogate an extended TCGA-derived GB patient population (n=146). non-parametric statistics, used to estimate the survival function from lifetime data of the 146 cases, produced a Kaplan-Meier plot identifying a low- and high-risk survival group, as shown in Figures 4E, F, whose molecular profile corresponded to the Resp and Non-Resp tumor groups, respectively (Figure 5F). As shown in Figure 5E, it is noteworthy that the Resp gene expression profile was associated exclusively with patients that belonged to the group of the longest survivors (>50 months).

To establish the type of GB molecular subtype to which our samples belong, we exploited a TCGA 490 gene expression profile deposited by the Anderson Cancer Center and created a classifier that allowed the assignment of each sample to one of the mesenchymal, classical, proneural, neural, and G-CIMP categories. As shown in Figure 5G, the Non-Resp group was mostly composed of samples of the mesenchymal type, which represents the most aggressive subtype (37) (Supplementary Table 7).

Whole exome analysis (WEA)

WEA was evaluated in 16 GB tumors divided into nine Non-Resp and seven Resp cases. The mutational landscape of Resp vs. Non-Resp is shown in Figures 6A, B. In Non-Resp samples, the mutational load was higher for any type of variant than in Resp cases (Figure 6A), as widely described in more aggressive and less TMZ-responsive tumor phenotypes (38). The distribution of base substitutions revealed a prevalence of T>G and C>T transversions in Non-Resp versus Resp tumors (Figure 6B).

We analyzed mutations in genes known to be altered in IDH1-WT GB by referring to the My Cancer Genome-MCG (mycancergenome.org database). We found 14 mutated genes in the 16 GB cases, for a total of 28 different variants (Figure 6C; Supplementary Figure 5, Supplementary Table 8). The analysis confirmed a higher mutational burden in the Non-Resp group with more deleterious alterations in the PTEN, RB1, and NF1 genes, which are well-known tumor suppressor genes in GB, indicating a more aggressive phenotype in accordance with our previous results (39).

Using Maftools forestPlot, we identified seven genes that significantly distinguished between the two groups of tumors (Figure 5D, Supplementary Figure 6, and Supplementary Table 9). Each variant is shown in detail in Supplementary Table 9. Two variants of FBN3, $FBN3^{E492K}$ in GB14 and $FBN3^{R2688Q}$ in GB16, have already been described and annotated in COSMIC with the IDs COSM9337963 and COSM3541504, respectively. The impact on protein function and thus clinical significance has not yet been annotated for most of these variants, resulting in "unknown significance" for the Varsome classification. Only the two splicing variants in DNAH5 in samples GB6c and in DENND6B in sample GB13 were predicted to be pathogenic. Three genes (ZNF713, DNAH5, and SLC7A4) were mutated only in the Non-Resp group (67% (6/9), 56% (5/9), and 56% (5/9), respectively). GALNTL5, FBN3, and DENND6B were shared only by the Resp group at a frequency of 56%. The OTOR gene was common between the groups of tumors, but with a higher mutation rate in Resp cases. To the best of our knowledge, none of the identified genes have been associated with glioblastoma.

CNApp (40) analysis was used to analyze chromosomal abnormalities in the 16 GB samples to uncover similarities and differences in copy number changes between tumors in the same group and between the two groups (Figures 6E, F). The most prominent chromosomal alteration, present in more than 50% of the samples in both the Resp and Non-Resp groups, involves both p and q arms of chromosomes 7, 9 and 10, specifically characteristic of IDH-WT GBs (41). Non-Resp tumors showed loss of chromosomes 13 and 14, while, interestingly, the Resp group shows complete chromosomal conservation (Figures 6E,

10.3389/fonc.2022.969812

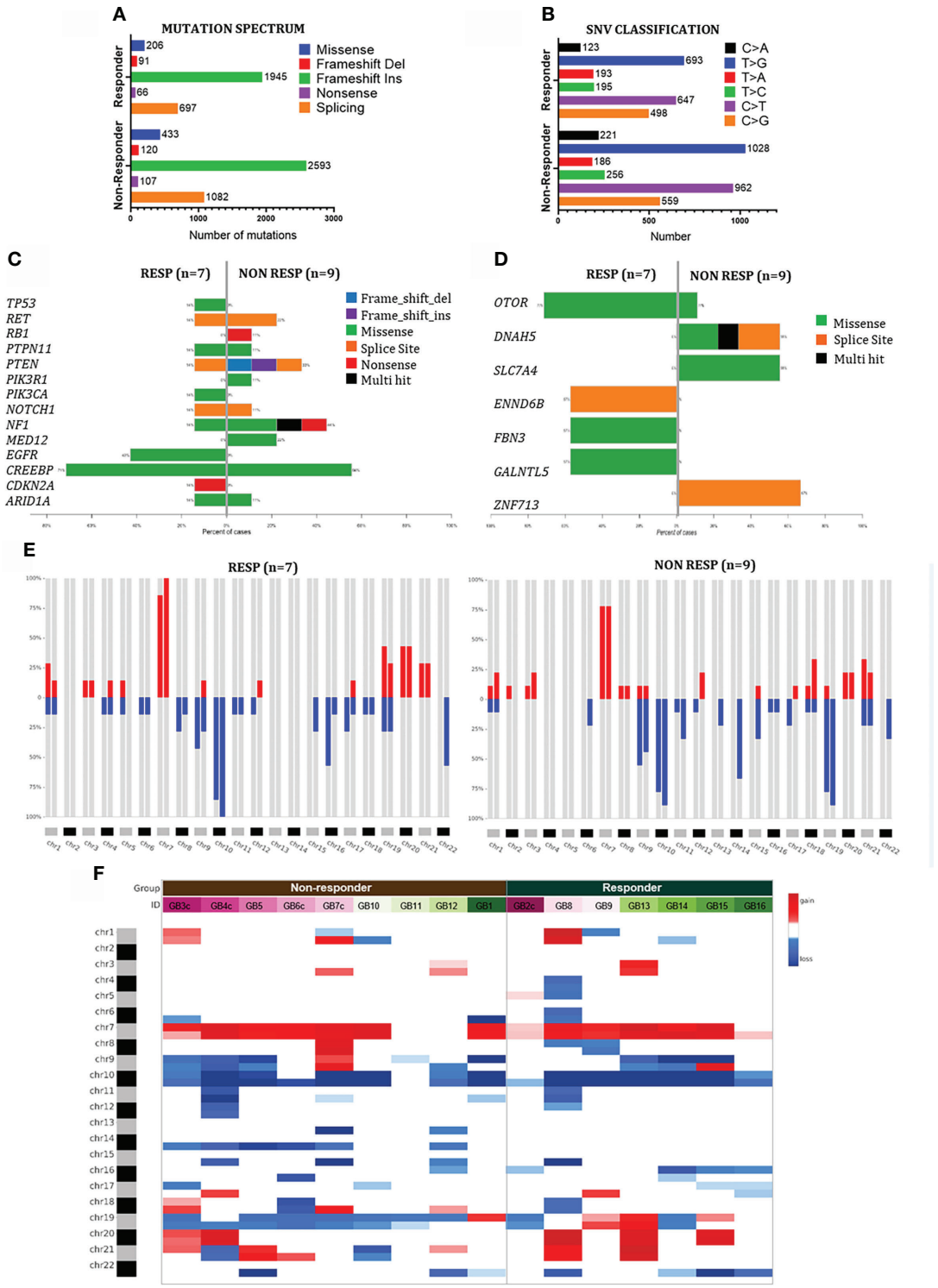

FIGURE 6
Mutational profiling of GB-EXPs. **(A, B)** The mutation landscape of the GB cohort (n=16). Counts of each variant classification **(a)** and counts of each single-nucleotide variant (SNV) classification **(B)**. **(C)** Co-bar plot of the most frequent gene mutations in GB. **(D)** Co-bar plot of the genes significantly discriminating Non-Resp and Resp groups. **(E)** CNApp frequencies for the p and q arms of each chromosome in Resp and Non-Resp groups. Alteration frequency is expressed as the percentage of altered samples out of the total within each group (red for gains and blue for losses). **(F)** Heatmap of individual copy number region profiles shows changes in copy number of chromosome regions between Resp (n=7) and Non.Resp (n=9) groups (red for chromosome gains and blue for losses).

F). Chromosome 14 has been described in GB patients as a carrier of several tumor suppressor genes (42). A gain of chromosomes 19 and 20 was observed in a higher percentage of tumors of the Resp group than in the Non-Resp group. Amplification of chromosome 19 has been identified as a favorable prognostic marker for GB (43). These results are indicative of a differential genetic background associated with the NAD(P)H FLIM-based TMZ response assessment, further confirming the validity of our approach.

Discussion

Glioblastoma is the most aggressive malignant tumor of the central nervous system and has a highly unfavorable prognosis. Despite the hardworking search for therapeutic strategies to reverse the highly unfavorable prognoses of GB patients, maximal surgery resection, standard temozolomide chemotherapy (TMZ) and radiotherapy (RT), while not resolutive, currently remain the best treatment option, unchanged since 2005 (3). This therapeutic standstill in the GB field is because, novel experimental approaches have shown limited success in improving patient survival (44). To date, preclinical ex vivo drug testing approaches have failed mainly because they do not respect the complexity of each individual glioblastoma cellular organization and composition (5). In this study, we have developed a novel approach to test the response to an anticancer treatment in patient-derived glioblastoma 3D organoids that we term GB-EXPs. The uniqueness of our approach is to avoid keeping the organoids in culture for extended time to prevent it from undergoing the usual genetic and morphological evolution and divergence from the tumor of origin. Many other *in vitro* glioblastoma organoid models (6, 8) consist of several weeks of culturing, wasting the patients' precious time who in the meantime progress in their short-term fatal clinical course. This long culture period is also due to the fact that conventional *in vitro* drug testing assays require very long application settings and readout times with various biological, molecular, genetic, and chemical assays (45), that inevitably lead to prolongation of *in vitro* tumor growth, which in the long term alters an already formed 3D tumor structure, such as a GB-EXP example.

Here we applied a metabolic imaging method that exploits the intrinsic auto-fluorescence molecular properties of NAD(P)H, a metabolic enzyme cofactor, that is associated with the metabolic state of the tissue. Studying intracellular metabolic shifts allows a precocious assessement of cellular response to treatment because anticipates any actual cellular behavior (11). In several recent studies, measurement of cancer cell metabolism by live imaging using intrinsic fluorescence from metabolic enzymatic cofactors such as NAD(P)H has shown promise as a sensitive non-invasive method for the early prediction of drug response (10, 27). Therefore, FLIM NAD(P)H, that does not require any type of staining, is perfectly suitable for GB-EXPs because it identifies, at an early stage of culturing, metabolic changes rapidly and non-invasively on the biological material used, leaving it vital (10) without interfering with its internal structure (27, 46). Our approach, therefore, overcomes the limitations of other *in vivo* drug testing tools since it allows to give a response to treatment after 72hr at the latest from initial treatment and within one week after surgery, allowing the tumor to remain viable and not diverge excessively from how it was structured *in vivo* in the patient, as shown in Figures 1K, L.

Skala et al. in 2017 implemented for the first time FLIM-based metabolic imaging as an ex-vivo drug testing tool on breast cancer organoids leveraging on NAD(P)H and FAD as metabolic intracellular biomarkers (27). Here we applied the same approach for the first time on glioblastoma organoids and unlike these authors we analyzed the FLIM measurements using the phasor data analysis approach, a mathematical method that is more suitable for a complex *in vitro* system such as cancer organoids (17). The phasor analysis approach allowed, through the segmentation of the mean distribution curves of the free/bound NAD(P)H fractions operated by the FLIM computational analysis system, the analysis of each tumor in its part and the evaluation of the different internal metabolic states. In such a way, we could calculate the percentage of drug response for each sample and refine the stratification of the tested tumor samples.

We used TMZ to validate the whole procedure. TMZ treatment was the first and only drug to which each GB tumor sample was exposed after first diagnosis. Each patient-derived tumor was classified as a TMZ Resp or Non-Resp sample. We could successfully corroborate our FLIM-based results using conventional drug testing methods and genomic and transcriptomic characterization analyses. In this validation process, a specific molecular status significantly distinguished the two TMZ Resp and Non-Resp tumor populations, stratified phenotypically solely by the NAD(P)H-FLIM based readouts. This distinction at the molecular level strengthens the accuracy of this approach. In fact, between the two groups of patient-derived tumors, which share many common characteristics of GB, we have been able to highlight, quite strikingly, markers already described in the literature, but also new potential targets associated with the response to TMZ, such as ANKRD28, PTPRD, ZNF713, DNAH5, SLC7A4, GALNTL5, FBN3, DENND6B, and OTOR. In particular, the accuracy of the NAD(P)H FLIM-based stratification could solve intra-tumor heterogeneity, confirmed by the different TMZ responses of GB3 and GB4 c and p portions (Figure 4G), which according to their phenotype had differential gene expression levels for several of the genes listed above, especially ANKRD28 and PTPRD that completely lost gene expression in the TMZ NR portions (Figure 5B). Furthermore, a unique new 17-gene expression signature significantly

discriminating the Resp and Non-Resp groups emerged. Since our tumor cases derived from patients for whom the clinical course was not yet available, we could not have a clinical confirmation of what was predicted *in vitro*. Therefore, in the meantime, we decided to test the tumor molecular profiles on a series of 150 patients of the glioblastoma TCGA dataset completely clinically characterized. This investigation revealed that the molecular profile that characterized our TMZ responsive and non-responsive tumor populations were highly significantly associated with the long-surviving and short surviving groups of the TCGA dataset, as we would predict. In depth studies are required to investigate the potential role of the 17 genes signature in glioblastoma.

Furthermore although MGMT methylation status is accepted as the only molecular prognostic biomarker for predicting patient response to TMZ treatment, inconsistencies do occur and currently challenge the efficacy of this biomarker in clinical practice, raising the question of its value (47). Here the number of methylated tumors for MGMT was higher in the responsive group than in the non-responsive group, as expected. However, following our procedure, some non-methylated tumor cases turned out to be nevertheless responsive to TMZ, suggesting that our approach could be synergistic with the classical MGMT methylation biomarker.

This study is the first to apply FLIM-based metabolic imaging to *in vitro* vital patient-derived GB tumors to perform an ex vivo treatment tumor response assessment early before losing the parental tumor architecture. The lack of predictive biomarkers is a major limitation in GB clinical oncology, and today, clinicians urgently need step-changing informative tools to support their decision-making therapy approaches. A method to predict a patient's tumor-specific drug response before the onset of therapy can be useful for managing patients with GB. This innovative approach in the field of glioblastoma can be transformative for the clinical management of the patients with glioblastoma, especially at the time of disease progression when the guidelines are less stringent and when the patient can receive more therapeutic options. The performance of such a functional precision medicine approach can provide additional information regarding a patient's tumor vulnerabilities. These functional approaches open the door to new discoveries and generate further knowledge of the disease, which in turn will increase the likelihood of producing useful therapeutic solutions (48). It is important to point out that the full promise of precision medicine in oncology is yet to be realized, as more individuals may benefit from functional approaches. In the glioblastoma clinical field, we envision an increasing implementation of functional precision medicine protocols and a transition from therapeutic approaches followed by watchful waiting to informed decisions based on specific patient-derived GB tumor treatment-response predictions. This approach can also be used to test new FDA-approved anti-cancer drugs *in vitro* directly on the tumor, could also be seen as a springboard for new drugs that need to be transferred to more advanced stages of clinical trials and be implemented for other cancers.

Data availability statement

The data presented in the study are deposited in the European Genome-Phenome Archive (https://ega-archive.org) and can be accessed using accession numbers PRJEB53727 and ERP138542.

Ethics statement

The studies involving human participants were reviewed and approved by Ethics Committee of the University Hospital of Pisa (787/2015). The patients/participants provided their written informed consent to participate in this study.

Author contributions

Conceived, designed and managed the project, wrote the paper, analyze the data CM; edited the paper, designed experiments, performed analyses, collected and analyzed data MM; performed experiments FL, SB, RL, and SF; collected human materials NM, PP, OS, CG, FPie, FA, and GL; pathological reports AN and PV; clinical data, ethical approval FPai, FPas, and AF; idea conceptualization, paper editing, MS, PM, and DO; data analysis PA; tissues processing MMe; FLIM methods optimizations GS, FC, and GF. All authors contributed to the article and approved the submitted version.

Funding

The study was supported by FPSgrant2018 from the Fondazione Pisana per la Scienza, Pisa, Italy.

Acknowledgments

We would like to thank Prof. Kevin Janes at the Department of Biomedical Engineering, University of Virginia, USA, for kindly providing us with OrganoSeg Software. We would also like to express our special thanks to Mr. Raffaele Cotugno for his kind donations to this project.

Conflict of interest

The authors declare that the research was conducted in the absence of any commercial or financial relationships that could be construed as a potential conflict of interest.

Publisher's note

All claims expressed in this article are solely those of the authors and do not necessarily represent those of their affiliated organizations, or those of the publisher, the editors and the reviewers. Any product that may be evaluated in this article, or claim that may be made by its manufacturer, is not guaranteed or endorsed by the publisher.

Supplementary material

The Supplementary Material for this article can be found online at: https://www.frontiersin.org/articles/10.3389/fonc.2022.969812/full#supplementary-material

References

1. Tan AC, Ashley DM, López GY, Malinzak M, Friedman HS, Khasraw M. Management of glioblastoma: State of the art and future directions. *CA Cancer J Clin* (2020) 70(4):299–312. doi: 10.3322/caac.21613

2. Le Calvé B, Rynkowski M, Le Mercier M, Bruyère C, Lonez C, Gras T, et al. Long-term *in vitro* treatment of human glioblastoma cells with temozolomide increases resistance *in vivo* through up-regulation of glut transporter and aldo-keto reductase enzyme akr1c expression 1. *Neoplasia.com.* (2010) 12:727–39. doi: 10.1593/neo.10526

3. Maher EA, Bachoo RM. Glioblastoma. *Rosenberg's Molecular and Genetic Basis of Neurological and Psychiatric Disease: Fifth Edition.* Boston: Academic Press (2014) p. 909–17. doi: 10.1016/B978-0-12-410529-4.00078-4

4. Butler M, Pongor L, Su YT, Xi L, Raffeld M, Quezado M, et al. MGMT status as a clinical biomarker in glioblastoma. *Trends Cancer* (2020) 6(5):380–91. doi: 10.1016/j.trecan.2020.02.010

5. Pinto B, Henriques AC, Silva PMA, Bousbaa H. Three-dimensional spheroids as *in vitro* preclinical models for cancer research. *Pharmaceutics* (2020) 12(12):1–38. doi: 10.3390/pharmaceutics12121186

6. Jacob F, Salinas RD, Zhang DY, Nguyen PTT, Schnoll JG, Wong SZH, et al. A patient-derived glioblastoma organoid model and biobank recapitulates inter- and intra-tumoral heterogeneity. *Cell* (2020) 180(1):188–204.e22. doi: 10.1016/j.cell.2019.11.036

7. Darrigues E, Zhao EH, De Loose A, Lee MP, Borrelli MJ, Eoff RL, et al. Biobanked glioblastoma patient-derived organoids as a precision medicine model to study inhibition of invasion. *Int J Mol Sci* (2021) 22(19). doi: 10.3390/ijms221910720

8. Stockslager MA, Malinowski S, Touat M, Yoon JC, Geduldig J, Mirza M, et al. Functional drug susceptibility testing using single-cell mass predicts treatment outcome in patient-derived cancer neurosphere models. *Cell Rep* (2021) 37(1):109788. doi: 10.1016/j.celrep.2021.109788

9. Cekanova M, Rathore K. Animal models of cancer utility and limitations. *Dev Ther* (2014) 8:1911–22. doi: 10.2147/DDDT.S49584

10. Lukina MM, Dudenkova VV, Ignatova NI, Druzhkova IN, Shimolina LE, Zagaynova EV, et al. Metabolic cofactors NAD(P)H and FAD as potential indicators of cancer cell response to chemotherapy with paclitaxel. *Biochim Biophys Acta - Gen Subj* (2018) 1862(8):1693–700. doi: 10.1016/j.bbagen.2018.04.021

11. Kolenc OI, Quinn KP. Evaluating cell metabolism through autofluorescence imaging of NAD(P)H and FAD. *Antioxidants Redox Signal* (2019) 30(6):875–89. doi: 10.1089/ars.2017.7451

12. Datta R, Heaster TM, Sharick JT, Gillette AA, Skala MC. Fluorescence lifetime imaging microscopy: Fundamentals and advances in instrumentation, analysis, and applications. *J BioMed Opt* (2020) 25(07):1. doi: 10.1117/1.jbo.25.7.071203

13. Trinh AL, Chen H, Chen Y, Hu Y, Li Z, Siegel E, et al. Tracking functional tumor cell subpopulations of malignant glioma by phasor fluorescence lifetime imaging microscopy of NAD(P)H. *Cancers (Basel)* (2017) 9(12):1–13. doi: 10.3390/cancers9120168

14. Foty R. A simple hanging drop cell culture protocol for generation of 3D spheroids. *J Vis Exp* (2011) 51. doi: 10.3791/2720

15. Erkkilä MT, Reichert D, Gesperger J, Kiesel B, Roetzer T, Mercea PA, et al. Macroscopic fluorescence-lifetime imaging of NAD(P)H and protoporphyrin IX improves the detection and grading of 5-aminolevulinic acid-stained brain tumors. *Sci Rep* (2020) 10(1). doi: 10.1038/s41598-020-77268-8

16. Ludtmann MHR, Angelova PR, Zhang Y, Abramov AY, Dinkova-Kostova AT. Nrf2 affects the efficiency of mitochondrial fatty acid oxidation. *Biochem J* (2014) 457(3):415–24. doi: 10.1042/BJ20130863

17. Ranjit S, Malacrida L, Jameson DM, Gratton E. Fit-free analysis of fluorescence lifetime imaging data using the phasor approach. *Nat Protoc* (2018) 13(9):1979–2004. doi: 10.1038/s41596-018-0026-5

18. Sharick JT, Walsh CM, Sprackling CM, Pasch CA, Pham DL, Esbona K, et al. Metabolic heterogeneity in patient tumor-derived organoids by primary site and drug treatment. *Front Oncol* (2020) 10:553. doi: 10.3389/fonc.2020.00553

19. Borten MA, Bajikar SS, Sasaki N, Clevers H, Janes KA. Automated brightfield morphometry of 3D organoid populations by OrganoSeg. *Sci Rep* (2018) 8(1):1–10. doi: 10.1038/s41598-017-18815-8

20. Walsh AJ, Cook RS, Sanders ME, Arteaga CL, Skala MC. Drug response in organoids generated from frozen primary tumor tissues. *Sci Rep* (2016) 6(June 2015):1–12. doi: 10.1038/srep18889

21. Lee SY. Temozolomide resistance in glioblastoma multiforme. *Genes Dis* (2016) 3(3):198–210. doi: 10.1016/j.gendis.2016.04.007

22. Kanzawa T, Germano IM, Kondo Y, Ito H, Kyo S, Kondo S. Inhibition of telomerase activity in malignant glioma cells correlates with their sensitivity to temozolomide. *Br J Cancer* (2003) 89(5):922–9. doi: 10.1038/sj.bjc.6601193

23. Yan Y, Xu Z, Chen X, Wang X, Zeng S, Zhao Z, et al. Novel function of lncrna adamts9-as2 in promoting temozolomide resistance in glioblastoma *via* upregulating the fus/mdm2 ubiquitination axis. *Front Cell Dev Biol* (2019) 7:217 (October). doi: 10.3389/fcell.2019.00217

24. Wang X, Wang Y, Zhang Z, Huang M, Fei Y, Ma J, et al. Discriminating different grades of cervical intraepithelial neoplasia based on label-free phasor fluorescence lifetime imaging microscopy. *BioMed Opt Express* (2020) 11(4):1977. doi: 10.1364/boe.386999

25. Skala MC, Riching KM, Bird DK, Gendron-Fitzpatrick A, Eickhoff J, Eliceiri KW, et al. *In vivo* multiphoton fluorescence lifetime imaging of proteinbound and free nad(p)h in normal and pre-cancerous epithelia. *J BioMed Opt.* (2007) 12(2):1–19. doi: 10.1117/1.2717503.In

26. Golebiewska A, Hau AC, Oudin A, Stieber D, Yabo YA, Baus V, et al. *Patient-derived organoids and orthotopic xenografts of primary and recurrent gliomas represent relevant patient avatars for precision oncology* Vol 140. Springer Berlin Heidelberg. doi: 10.1007/s00401-020-02226-7

27. Walsh AJ, Cook RS, Sanders ME, Gennaro C, Arteaga CL, Skala MC. Quantitative optical imaging of primary tumor organoid metabolism predicts drug response in breast cancer. *Cancer Res* (2014) 74(18):5184–94. doi: 10.1158/0008-5472.CAN-14-0663

28. Bastola S, Pavlyukov MS, Yamashita D, Ghosh S, Cho H, Kagaya N, et al. Glioma-initiating cells at tumor edge gain signals from tumor core cells to promote their malignancy. *Nat Commun* (2020) 11(1):1–17. doi: 10.1038/s41467-020-18189-y

29. Radke J, Koch A, Pritsch F, Schumann E, Misch M, Hempt C, et al. Predictive MGMT status in a homogeneous cohort of IDH wildtype glioblastoma patients. *Acta Neuropathol Commun* (2019) 7(1):89. doi: 10.1186/s40478-019-0745-z

30. Areeb Z, Stuart SF, West AJ, Gomez J, Nguyen HPT, Paradiso L, et al. Reduced EGFR and increased miR-221 is associated with increased resistance to temozolomide and radiotherapy in glioblastoma. *Sci Rep* (2020) 10(1):1–12. doi: 10.1038/s41598-020-74746-x

31. Xu X, Wang Z, Liu N, Cheng Y, Jin W, Zhang P, et al. Association between SOX9 and CA9 in glioma, and its effects on chemosensitivity to TMZ. *Int J Oncol* (2018) 53(1):189–202. doi: 10.3892/ijo.2018.4382

32. Kipper FC, Silva AO, Marc AL, Confortin G, Junqueira AV, Neto EP, et al. Vinblastine and antihelmintic mebendazole potentiate temozolomide in resistant gliomas. *Invest New Drugs* (2018) 36(2):323–31. doi: 10.1007/s10637-017-0503-7

33. Wang D, Berglund A, Kenchappa RS, Forsyth PA, Mule JJ, Etame AB. BIRC3 is a novel driver of therapeutic resistance in glioblastoma. *Sci Rep* (2016) 6 (October 2015):1–13. doi: 10.1038/srep21710

34. Frazzi R. BIRC3 and BIRC5: multi-faceted inhibitors in cancer. *Cell Biosci* (2021) 11(1):0–14. doi: 10.1186/s13578-020-00521-0

35. Skiriute D, Steponaitis G, Vaitkiene P, Mikučiunas M, Skauminas K, Tamašauskas A, et al. Glioma malignancy-dependent NDRG2 gene methylation and downregulation correlates with poor patient outcome. *J Cancer* (2014) 5 (6):446–56. doi: 10.7150/jca.9140

36. Veeriah S, Brennan C, Meng S, Singh B, Fagin JA, Solit DB, et al. The tyrosine phosphatase PTPRD is a tumor suppressor that is frequently inactivated and mutated in glioblastoma and other human cancers. *Proc Natl Acad Sci USA* (2009) 106(23):9435–40. doi: 10.1073/pnas.0900571106

37. Zhang P, Xia Q, Liu L, Li S, Dong L. Current opinion on molecular characterization for GBM classification in guiding clinical diagnosis, prognosis, and therapy. *Front Mol Biosci* (2020) 7:562798(September). doi: 10.3389/fmolb.2020.562798

38. Wang L, Ge J, Lan Y, Shi Y, Luo Y, Tan Y, et al. Tumor mutational burden is associated with poor outcomes in diffuse glioma. *BMC Cancer* (2020) 20(1):1–12. doi: 10.1186/s12885-020-6658-1

39. McDonald KL, Tabone T, Nowak AK, Erber WN. Somatic mutations in glioblastoma are associated with methylguanine-DNA methyltransferase methylation. *Oncol Lett* (2015) 9(5):2063–7. doi: 10.3892/ol.2015.2980

40. Franch-Expósito S, Bassaganyas L, Vila-Casadesús M, Hernández-Illán E, Esteban-Fabró R, Díaz-Gay M, et al. CNApp, a tool for the quantification of copy number alterations and integrative analysis revealing clinical implications. *Elife* (2020) 9. doi: 10.7554/eLife.50267

41. Mirchia K, Sathe AA, Walker JM, Fudym Y, Galbraith K, Viapiano MS, et al. Total copy number variation as a prognostic factor in adult astrocytoma subtypes. *Acta Neuropathol Commun* (2019) 7(1):92. doi: 10.1186/s40478-019-0746-y

42. Hu J, Jiang C, NG H, Pang JCS, Tong CYK. Chromosome 14q may harbor multiple tumor suppressor genes in primary glioblastoma multiforme. *Chin Med J* (2002) 115(8):1201–4.

43. Geisenberger C, Mock A, Warta R, Rapp C, Schwager C, Korshunov A, et al. Molecular profiling of long-term survivors identifies a subgroup of glioblastoma characterized by chromosome 19/20 co-gain. *Acta Neuropathol* (2015) 130(3):419–34. doi: 10.1007/S00401-015-1427-Y

44. Aldape K, Brindle KM, Chesler L, Chopra R, Gajjar A, Gilbert MR, et al. Challenges to curing primary brain tumours. *Nat Rev Clin Oncol* (2019) 16 (8):509–20. doi: 10.1038/s41571-019-0177-5

45. Hughes JP, Rees SS, Kalindjian SB, Philpott KL. Principles of early drug discovery. *Br J Pharmacol* (2011) 162(6):1239–49. doi: 10.1111/j.1476-5381.2010.01127.x

46. Ouyang Y, Liu Y, Wang ZM, Liu Z, Wu M. FLIM as a promising tool for cancer diagnosis and treatment monitoring. *Nano-Micro Lett* (2021) 13(1). doi: 10.1007/s40820-021-00653-z

47. Butler M, Pongor L, Su Y-T, Xi L, Raffeld M, Quezado M, Trepel J, Aldape K, Pommier YWJ. MGMT status as a clinical biomarker in glioblastomaitle. *Trends Cancer* (2020) 6(5):380–91. doi: 10.1016/j.trecan.2020.02.010

48. Letai A, Bhola P, Welm AL. Functional precision oncology: Testing tumors with drugs to identify vulnerabilities and novel combinations. *Cancer Cell* (2022) 40(1):26–35. doi: 10.1016/j.ccell.2021.12.004

COPYRIGHT

© 2022 Morelli, Lessi, Barachini, Liotti, Montemurro, Perrini, Santonocito, Gambacciani, Snuderl, Pieri, Aquila, Farnesi, Naccarato, Viacava, Cardarelli, Ferri, Mulholland, Ottaviani, Paiar, Liberti, Pasqualetti, Menicagli, Aretini, Signore, Franceschi and Mazzanti. This is an open-access article distributed under the terms of the Creative Commons Attribution License (CC BY). The use, distribution or reproduction in other forums is permitted, provided the original author(s) and the copyright owner(s) are credited and that the original publication in this journal is cited, in accordance with accepted academic practice. No use, distribution or reproduction is permitted which does not comply with these terms.